Electronic Supplementary Information

Promoting effects of $Ce_{0.75}Zr_{0.25}O_2$ on $La_{0.7}Sr_{0.3}MnO_3$ electrocatalyst for oxygen reduction reaction in metal-air batteries**

Yejian Xue[a], He Miao[a] *, Baihai Li[b], Shanshan Sun[a], Qin Wang[a], Shihua Li[a], Liang Chen[c] and Zhaoping Liu[a] *

[a] **Advanced Li-ion Battery Engineering Laboratory and Key Laboratory of Graphene Technologies and Applications of Zhejiang Province, Ningbo Institute of Materials Technology & Engineering, Chinese Academy of Sciences, Zhejiang 315201, P. R. China**

[b] **School of Energy Science and Engineering, University of Electronic Science and Technology of China, Chengdu 611731, P. R. China**

[c] **Ningbo Institute of Materials Technology & Engineering, Chinese Academy of Sciences, Zhejiang 315201, P. R. China.**

***E-mail: liuzp@nimte.ac.cn, hmiao@nimte.ac.cn**

Experimental Section

1 Materials and Methods

Lanthanum nitrate, strontium nitrate, manganese nitrate, zirconium nitrate, cerium nitrate, ammonium hydroxide and citric acid were purchased from Sinopharm Chemical Reagent Co. Ltd. Vulcan XC72 carbon was purchased from Cabot Corp. The Pt/C catalyst (20wt% Pt on Vulcan XC72R carbon) was purchased from Johnson Matthey Corporation. The composite catalyst of $Ce_{0.75}Zr_{0.25}O_2$-around-$La_{0.7}Sr_{0.3}MnO_3$ (LSM-CZ) was synthesized by two-step solution method. Firstly, the LSM material was synthesized by sol-gel method using citric acid as the chelating agent [1]. The LSM powder was obtained by the calcination of the dried gels at 950 ^oC for 2h. Then, the LSM powers, zirconium nitrate and cerium nitrate were mixed in beaker using water as the solvent. The ammonium hydroxide was put into a burette and allowed to drop into the slurry by the gentle stirring until the pH reaches 9. After being stirred for 1 hour, the resulting slurry was transferred into a 100 ml Teflon-Lined stainless steel autoclave and reacted at 110 ^oC for 24 h. When the reaction finished, the solution was cooled down to room temperature naturally and centrifuged to obtain the black composite material precursor. Subsequently, the precursor was washed with deionized water and dried in a muffle at 80 ^oC for 24 hours. Lastly, the LSM-CZ composite was obtained through annealing the dried precursor at 500 ^oC for 2 h with a heating rate of 100 $^oC\ h^{-1}$ in the air atmosphere.

2 Material characterizations

The structures and morphologies of LSM, CZ and LSM-CZ were investigated by means of X-ray diffraction (XRD), scanning electron microscopy (SEM) and transmission electron microscopy (TEM), respectively. The XRD patterns were measured in reflection

mode with a Cu K_α radiation source at a step of 0.02° in the range of 2θ from 10° to 90° on Bruker AXS D8 Advance. The SEM measurements were performed on FEI SIRION 200 instrument. The TEM micrographs were recorded with Tecnai F20 transmission electron microscope. In addition, the porous features and Brunauer-Emmett-Teller (BET) specific surface areas of the different samples were tested on ASAP 2020M (Micromertics Instrument Corp.), and the X-ray Photoelectron Spectroscopy (XPS) spectra were recorded by using ESCALAB 250 spectrometer with a mono X-Ray source Al Kα excitation (1486.6 eV). All the XPS spectra were calibrated with C1s peak at 284.8 eV from the universal hydrocarbon contamination. The oxygen adsorption behaviors of the different samples were also measured by Temperature Programmed Desorption (TPD, AutoChem II 2920, Micromeritics). Specifically, the samples (about 200 mg) placed in a quartz reactor was pretreated in O_2 (3%)/He (50 ml (STP) min^{-1}) at the temperature of 500 ^oC for 2 hours to remove the dissociative water and carbonate. Subsequently, the sample was cooled down to room temperature and then heated to 900 ^oC (5 ^oC min^{-1}) in He atmosphere (50 ml (STP) min^{-1}).

3 Oxygen reduction reaction (ORR) measurements

The catalytic activities toward ORR of LSM, CZ and LSM-CZ were studied by the rotating ring-disk electrode (RRDE) (Pine, American) technique. The RRDE measurements were performed by a three-electrode system in 0.1 M KOH electrolyte solution. Pt wire and Hg/HgO electrode were served as the counter and reference electrodes, respectively. The working electrode was a catalyst-coated RRDE (Pt ring and glass carbon (GC) disk, disk diameter: 5.6 mm, ring: 6.25~7.92 mm, current collection efficiency: 37%). The disk potential was scanned from 0.2 to -0.8 V (vs. Hg/HgO) at the

scan speed of 5 mV s^{-1}, and the potential of Pt ring electrode was held at 0.5 V (vs. Hg/HgO). Prior to measurement, O_2 was bubbled directly into the electrolytic cell for at least 30 min to saturate the solution with pure O_2 at a flow rate of 25 sccm. During the measurement, O_2 atmosphere was maintained. The onset potentials were taken from linear sweep voltammetry curves (LSVs) at the current density of 100 μA cm^{-2}. The cyclic voltammetry (CV) was also investigated on a rotating ring-disk electrode (RRDE) in an O_2-saturated or N_2-saturated 0.1 M KOH solution. Electrochemical impedance spectra (EIS) were recorded in the frequency range from 100 kHz to 0.01 Hz with an AC signal amplitude of 5 mV. Before the test, The Hg/HgO electrode was calibrated with respect to reversible hydrogen electrode (RHE). The calibration was performed in the 0.1 M KOH electrolyte saturated the high purity hydrogen with a platinum foil (3×3 cm^2) as the working electrode. The CV curve was cycled at a scan rate of 1 mV s^{-1}, and the average of the two potentials at which the current crossed zero, which was taken to be the thermodynamic potential for the hydrogen electrode reaction. So in 0.1 M KOH, $E_{(RHE)} = E_{(Hg/HgO)} + 0.923$ V (Figure S5). The catalyst ink was made from the suspension of sample (10 mg), 10 mg Vulcan XC72, 160 μL of Nafion solution (5 wt. %) and 2 mL of alcohol. Then, the suspension was dispersed by the ultrasound method for 30 minutes. Finally, 12.5 μL ink was dropped onto the working electrode of glassy carbon with the catalyst loading being approximately 0.236 mg cm^{-2}. The as-prepared electrodes were dried at room temperature for overnight.

All the experiments were tested at ambient condition. The Koutechy-Levich (K-L) plots were analyzed at different electrode potentials. The K-L plots can be expressed by the following equations (1) and (2)[2,3]:

$$j^{-1} = j_L^{-1} + j_K^{-1} = (B\omega^{1/2})^{-1} + j_K^{-1} \quad (1)$$

$$B = 0.62nFC_0(D_0)^{2/3}\nu^{-1/6} \quad (2)$$

Where j is the measured current density, j_K and j_L are the kinetic and diffusion-limiting current densities, respectively, ω is the angular velocity of the disk, n is the overall number of electrons transferred in the oxygen reduction, F is the Faraday constant (96485 C mol^{-1}), C_0 is O_2 volume concentration (1.2×10^{-6} mol cm^{-3}), υ is the kinematic viscosity of the electrolyte (0.01 cm^2 s^{-1}), and D_0 is the diffusion coefficient of O_2 in 0.1M KOH (1.9×10^{-5} cm^2 s^{-1}). In addition, from the RRDE LSV curves, the percentage of formed peroxides (HO_2^-) with respect to the total oxygen reduction products ($X_{HO_2^-}$) can be calculated by the disk current (J_{disk}), the ring current (J_{ring}) and the ring collection efficiency(N) with the equation (3) [4,5]:

$$X_{HO_2^-}[\%] = 100\frac{\frac{2J_{ring}}{N}}{J_{disk} + \frac{J_{ring}}{N}} \quad (3)$$

For the Tafel plot, the kinetic current was calculated as follows (the equation (4)):

$$j_K = \frac{j \times j_L}{j_L - j} \quad (4)$$

The catalysts of LSM-CZ, CZ, LSM and commercial Pt/C were analyzed by the chronoamperometric measurements at -0.5 V (vs. Hg/HgO) in O_2- saturated 0.1 M KOH at the rate of 1600 rpm for 100000 second, and the potential of Pt ring electrode was also held at 0.5 V.

4 Magnesium/Aluminum air battery measurements

Magnesium/Aluminum-air batteries were fabricated for testing the electrochemical performance on a multichannel battery testing system (CT2001A, Land Company). The as-synthesized LSM-CZ and LSM were used as the ORR catalysts. The cathode was fabricated with a three-layer structure including the catalyst layer, gas diffusion layer and current collector layer. The current collector layer and the gas diffusion layer were nickel foam and porous PTFE film with a square area (4 cm×4 cm), respectively. The catalytic layer was prepared in the following sequence: (i) as-prepared perovskite catalyst (0.36 g) and VXC-72 (0.36 g) were mixed in 50 ml ethanol to obtain a homogeneous solution, and then the solution was stirred magnetically in a beaker; (ii) 0.5 g PTFE emulsion (60 wt%) was added into the solution and stirred for further 30 minutes; (iii) the beaker was then transferred into an 80 ℃ water-bath with stirring until the ethanol was evaporated and the slurry formed a paste; (iv) the paste was rolled into a 0.35 mm of film with a square area of 4 cm × 4 cm. The catalytic layer was placed on the nickel foam, and pressed with a pressure of 20 MPa for 2 minutes, followed by the sintering at 340 ^{o}C for 30 minutes. Then, the above two-layer architecture was placed on the porous PTFE film, and pressed with a pressure of 10 MPa for 2 minutes at the temperature of 150 ^{o}C. Magnesium/Aluminum-air batteries were fabricated by using the as-prepared air cathodes and tested by a homemade testing device. For magnesium-air batteries, a magnesium alloy plate (AZ61) with an active area of 2×2 cm^2 and 10 wt% NaCl aqueous solution were used as the anode and electrolyte, respectively. For aluminum-air batteries, a high pure aluminum (99.99%) plate with an active area of 2×2 cm^2 and 4 mol L^{-1} KOH aqueous solution were used as the anode and electrolyte, respectively.

5 Computational Methods

First-principles calculations were performed by using the Vienna Ab *initio* Simulation Package (VASP).[6] The projector-augmented-wave (PAW) potentials[7] were used for the treatment of the core electrons. The electron exchange correlation interactions were treated within the generalized gradient approximation (GGA) using the Perdew-Burke-Ernzerhof (PBE) functional.[8] In order to correctly treat the strong correlation effects in the system, the DFT+U methods were adopted, in which the U_{eff}=3.9 and 5.0 for Mn and Ce, respectively. The magnetic order in $LaMnO_3$ was set to be A-type. To avoid the interactions between the slabs along the vertical direction, a vacuum layer with the total thickness of 30 Å was set in the supercell. The energy cutoff was set to 480 eV and a tolerance of no more than 0.02 eV/Å on each atom was used for convergence criterion. The Monkhorst-Pack[9] k-points sampling of 6×3×1 was utilized.

References

[1] J. X. Wang, J. L. Sun, C. R. He, Q. Wang, W. G. Wang, Journal of Power Sources 253 (2014) 424-430

[2] T. J. Schmidt, V. Stamenkovic, P. N. Ross, Jr. and N. M. Markovic, Phys. Chem. Chem. Phys. 5(2003) 400-406

[3] J. Hua, L. Wang, L. Shi, H. Huang, Electrochimica Acta 161 (2015) 115-123

[4] J. Suntivich, H. A. Gasteiger, N. Yabuuchi, Y. Shao-Horn, Journal of The Electrochemical Society 157(8)(2010) B1263-B1268

[5] J. Chen, N. Zhou, H. Wang, Z. Peng, H. Li, Y. Tang, K. Liu, Chem. Commun. 51(2015) 10123-10126

[6] Kresse, G.; Hafner, J. Phys. Rev. B 1993, 48, (17), 13115-13118.

[7] Blochl, P. E. Phys. Rev. B 1994, 50, (24), 17953-17979.

[8] Perdew, J.; Chevary, J. A.; Vosko, S. H.; Jackson, K.; Pederson, M.; Singh, D. J.; Fiolhais, C. Phys. Rev. B 1992, 46, (11), 6671-6687.

[9] Monkhorst, H. J.; Pack, J. D. Phys. Rev. B 1976, 13, 5188.

Support Scheme, Figure and Table Section

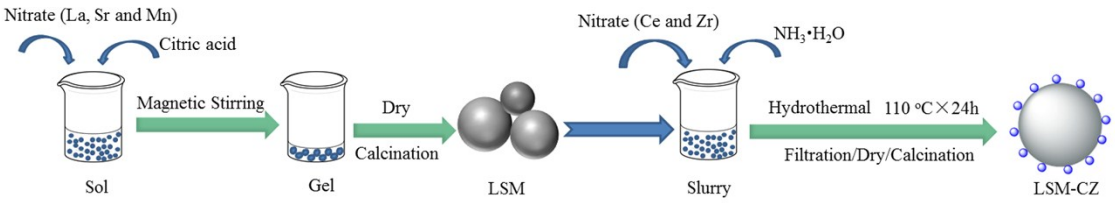

Scheme S1. LSM-CZ prepared by a two-step solution method.

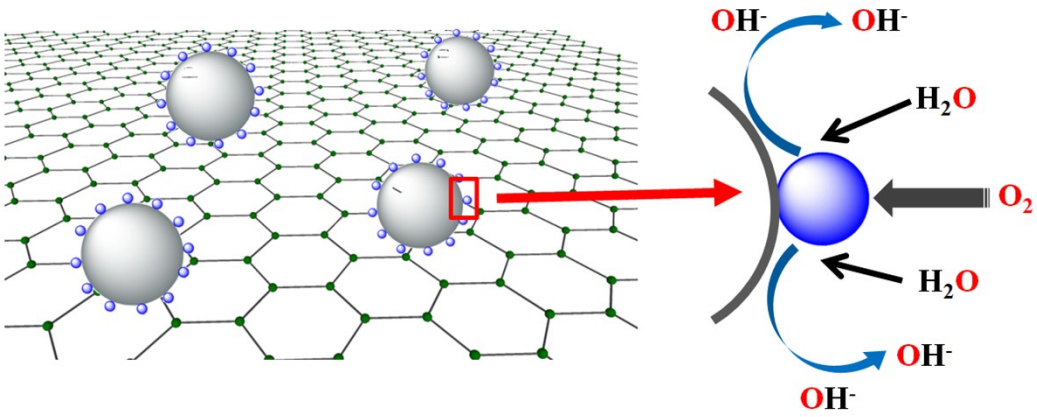

Scheme S2. Schematic diagram of ORR catalytic mechanism of LSM-CZ composite catalysts.

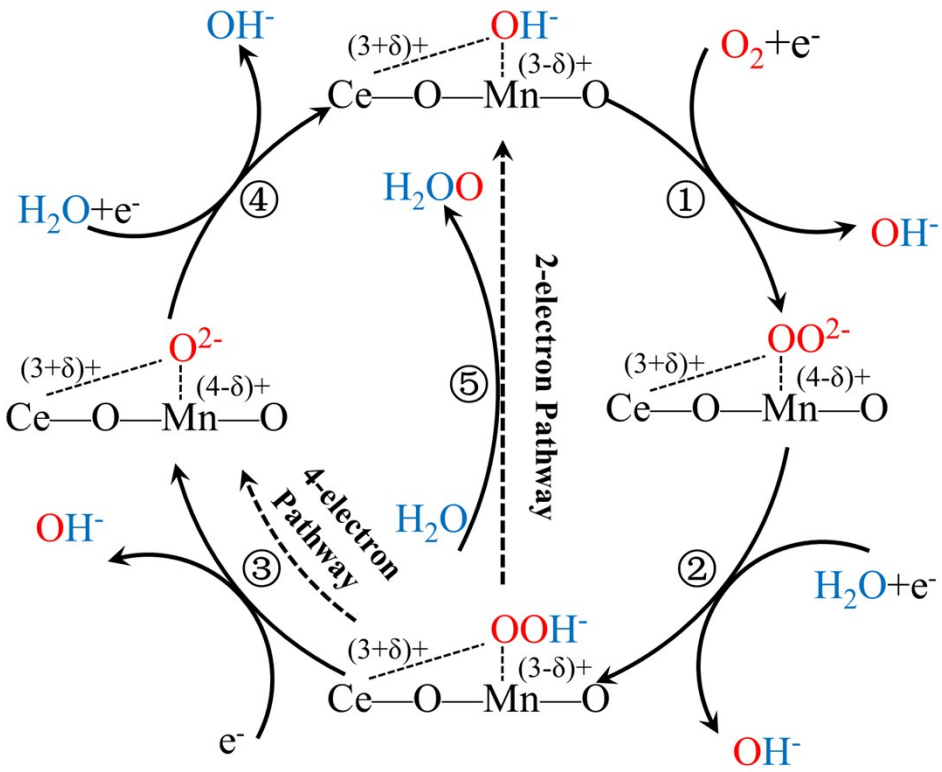

Scheme S3. Schematic of ORR catalytic mechanism of LSM-CZ composite catalysts.

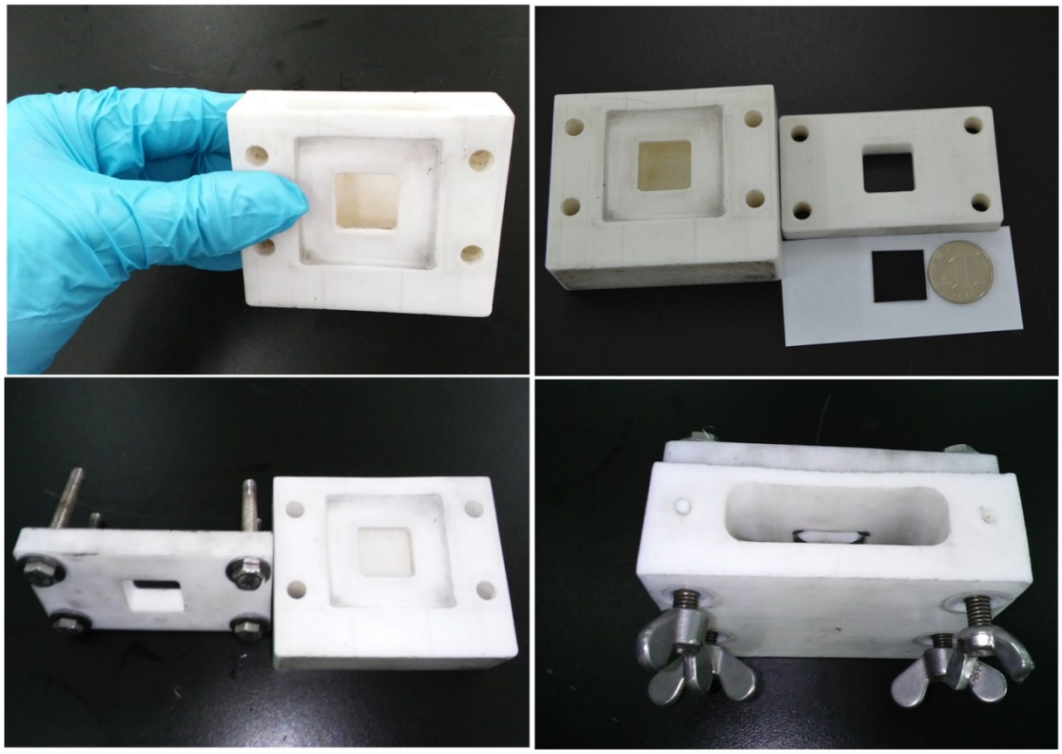

Figure S1. Homemade testing house and battery assembly.

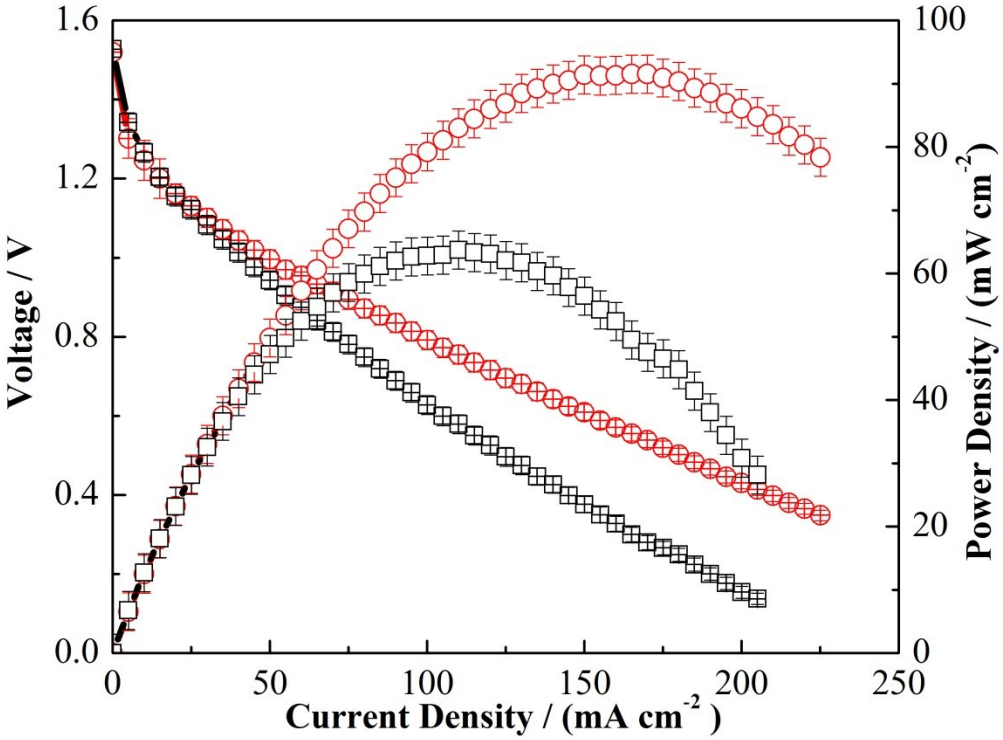

Figure S2. I-V and I-P curves of the Mg-air batteries with LSM (□) and LSM-CZ (○) catalysts. Active area: 2cm×2cm; Anode: AZ61; electrolyte: 10 wt% NaCl.

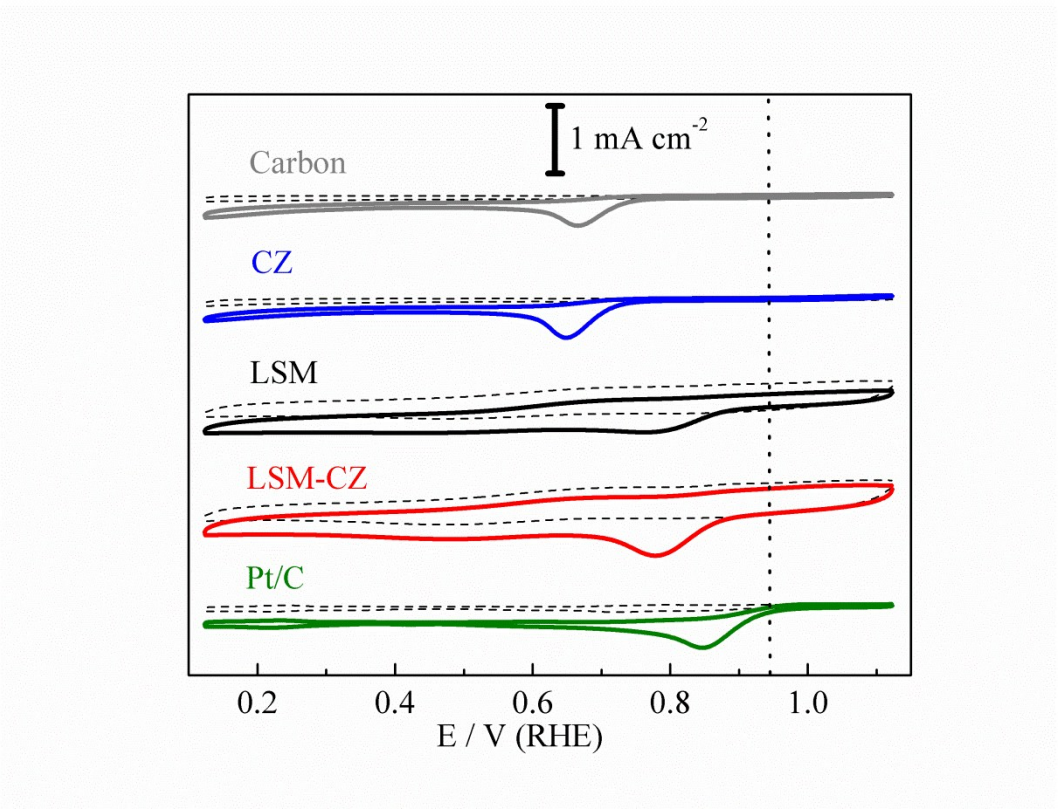

Figure S3. CV curves of Carbon, CZ, LSM, LSM-CZ and Pt/C catalysts in N_2/O_2-saturated 0.1M KOH at a sweep rate of 5 mV S^{-1}.

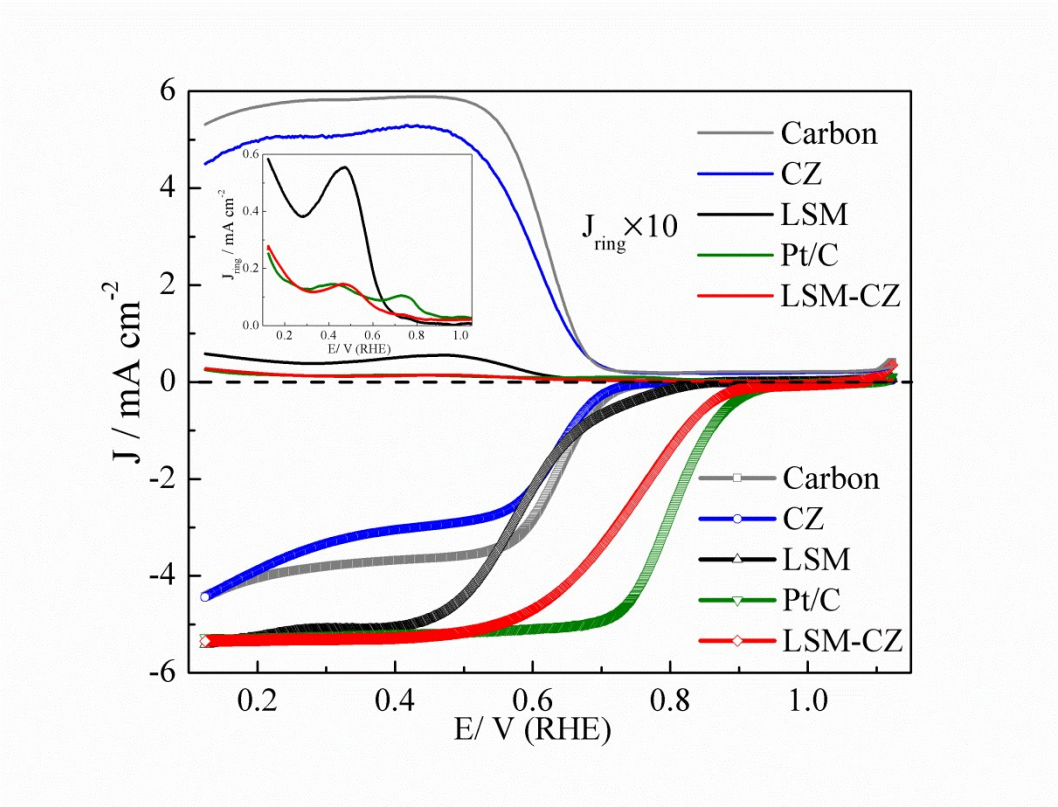

Figure S4. LSV curves and ring currents of Carbon, CZ, LSM, LSM-CZ and Pt/C catalysts in O_2-saturated 0.1M KOH at 1600 rpm at a sweep rate of 5 mV S^{-1}.

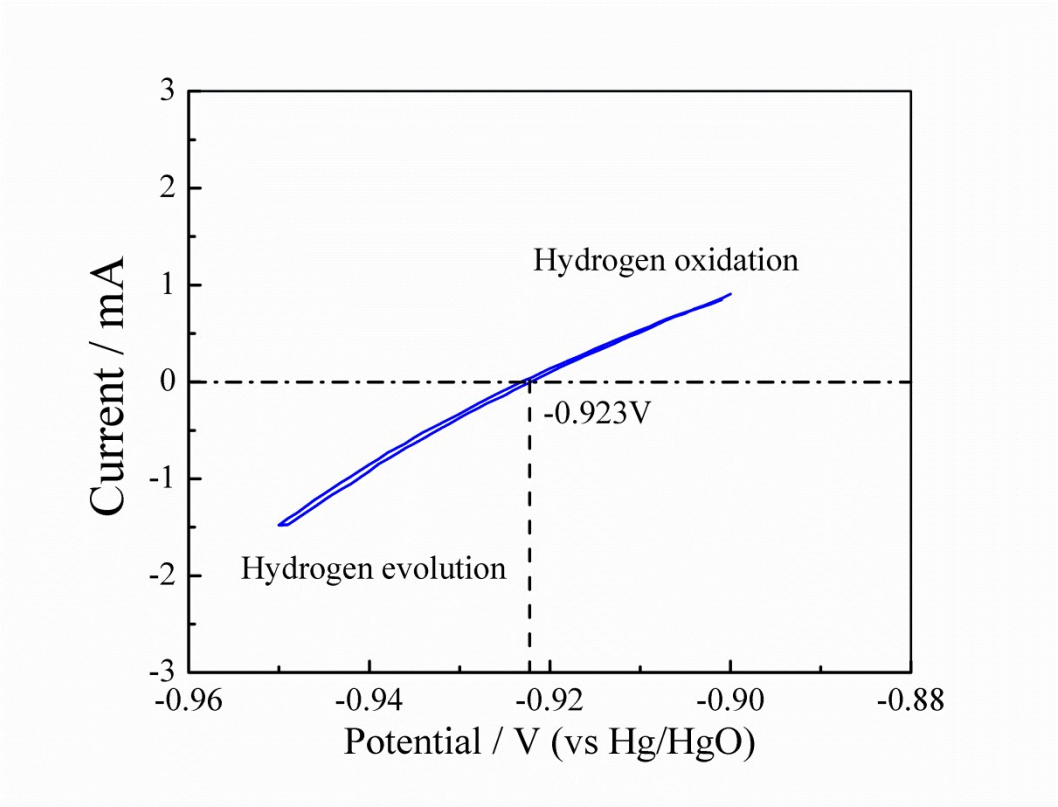

Figure S5. CV curve of the Hg/HgO electrode calibrated with respect to RHE.

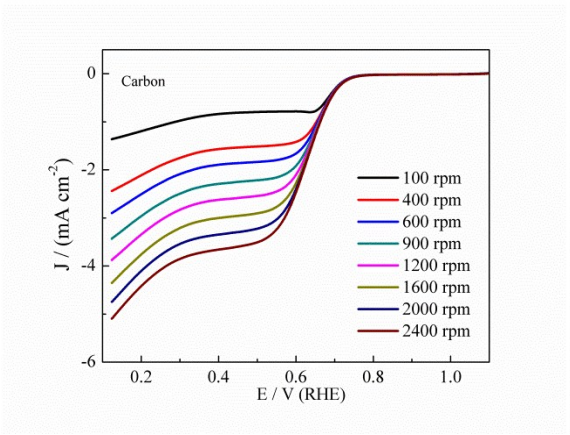
Carbon
100 rpm
400 rpm
600 rpm
900 rpm
1200 rpm
1600 rpm
2000 rpm
2400 rpm
J / (mA cm-2)
E / V (RHE)

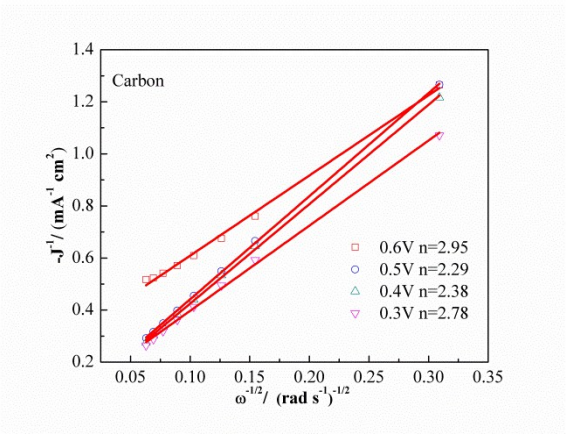
Carbon
0.6V n=2.95
0.5V n=2.29
0.4V n=2.38
0.3V n=2.78
-J-1/ (mA-1 cm2)
ω-1/2/ (rad s-1)-1/2

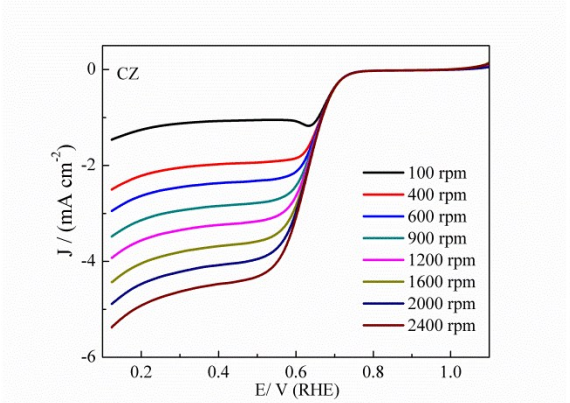
CZ
100 rpm
400 rpm
600 rpm
900 rpm
1200 rpm
1600 rpm
2000 rpm
2400 rpm
J / (mA cm-2)
E/ V (RHE)

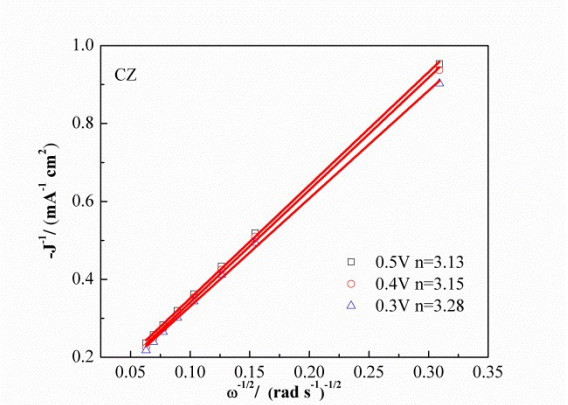
CZ
0.5V n=3.13
0.4V n=3.15
0.3V n=3.28
-J-1/ (mA-1 cm2)
ω-1/2/ (rad s-1)-1/2

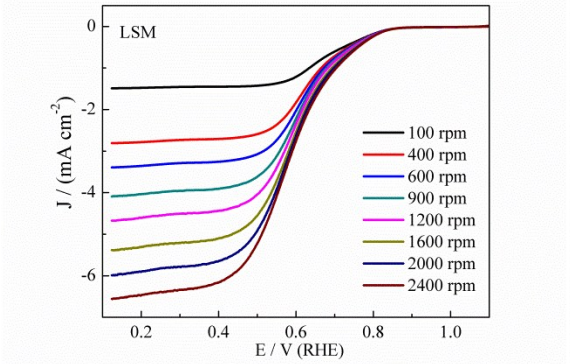
LSM
100 rpm
400 rpm
600 rpm
900 rpm
1200 rpm
1600 rpm
2000 rpm
2400 rpm
J / (mA cm-2)
E / V (RHE)

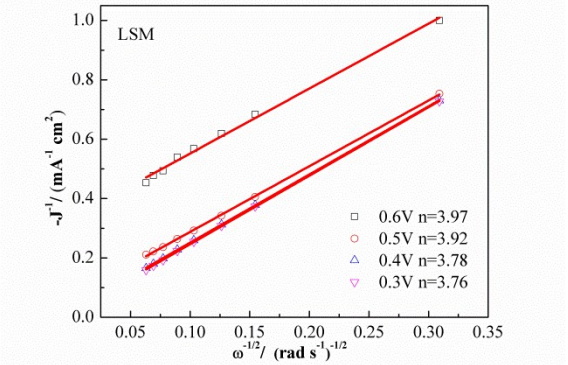
LSM
0.6V n=3.97
0.5V n=3.92
0.4V n=3.78
0.3V n=3.76
-J-1/ (mA-1 cm2)
ω-1/2/ (rad s-1)-1/2

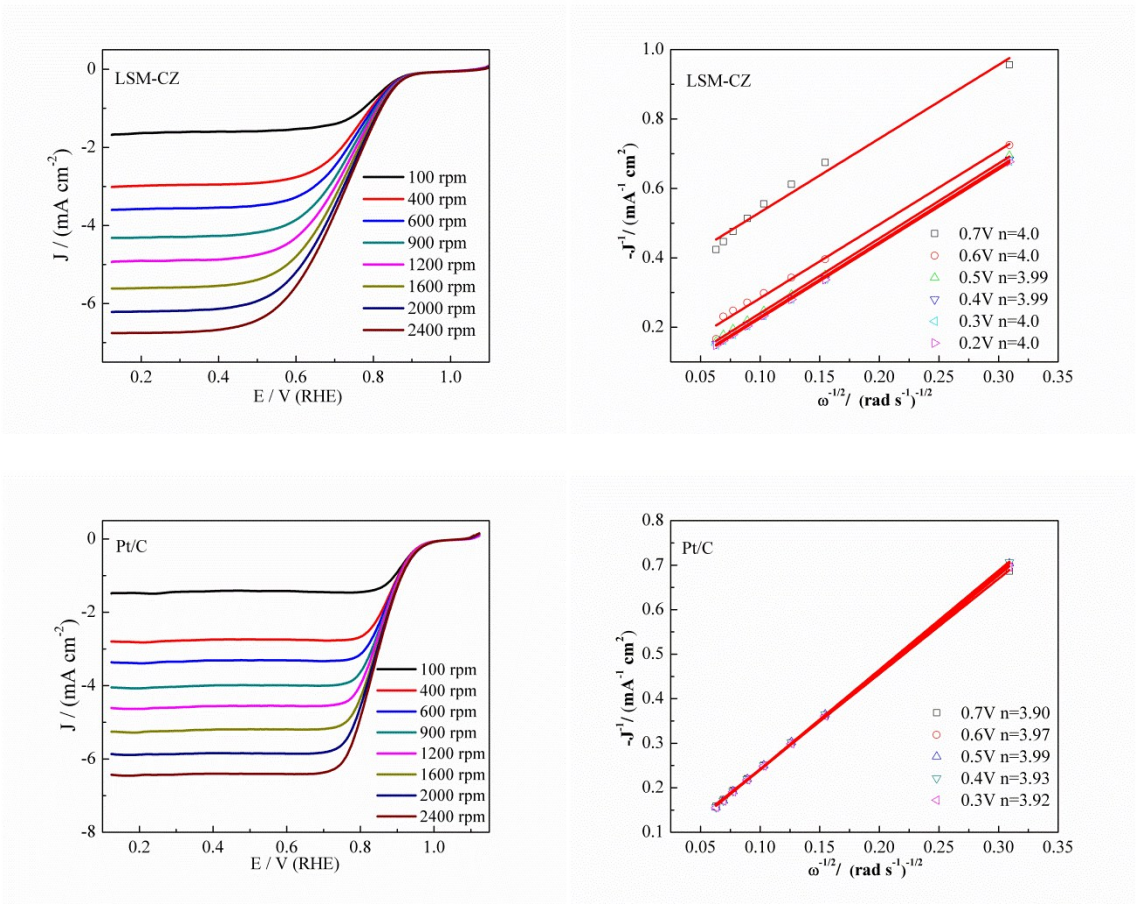

Figure S6. LSV curves at the different rotation rates and *n* values calculated by K-L equation of Carbon, CZ, LSM, LSM-CZ and Pt/C catalysts

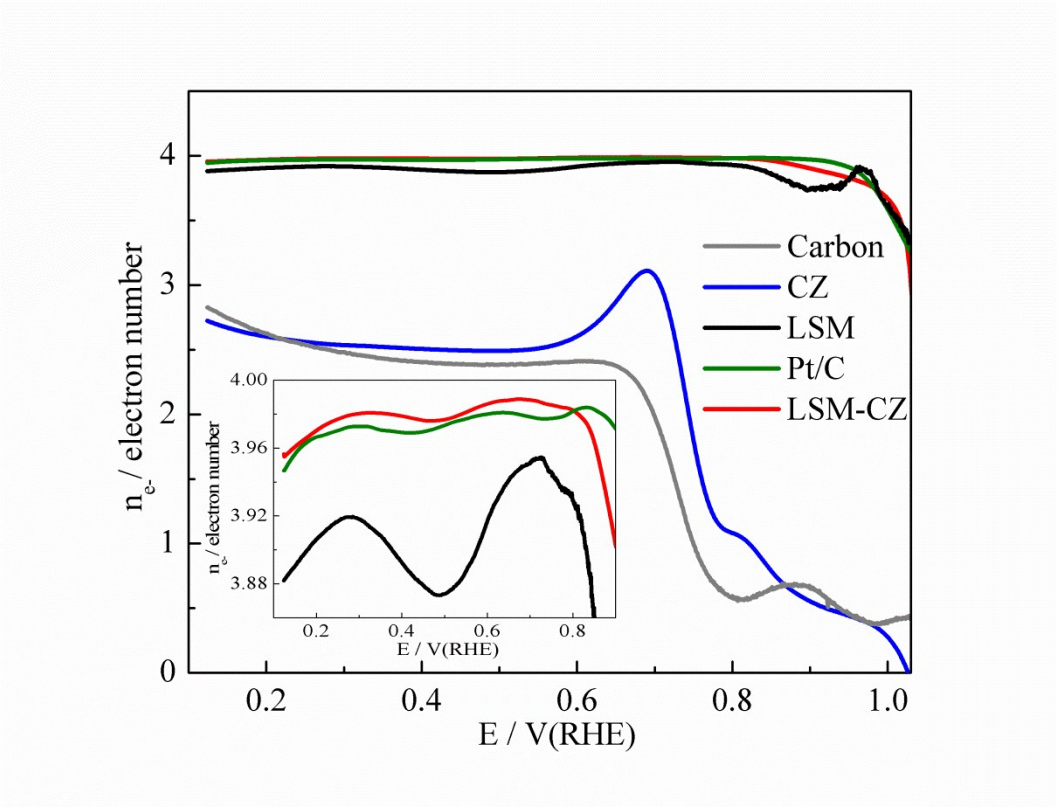

Figure S7. Overall numbers of transferred electrons (n_{e^-}) of Carbon, CZ, LSM, LSM-CZ and Pt/C catalysts.

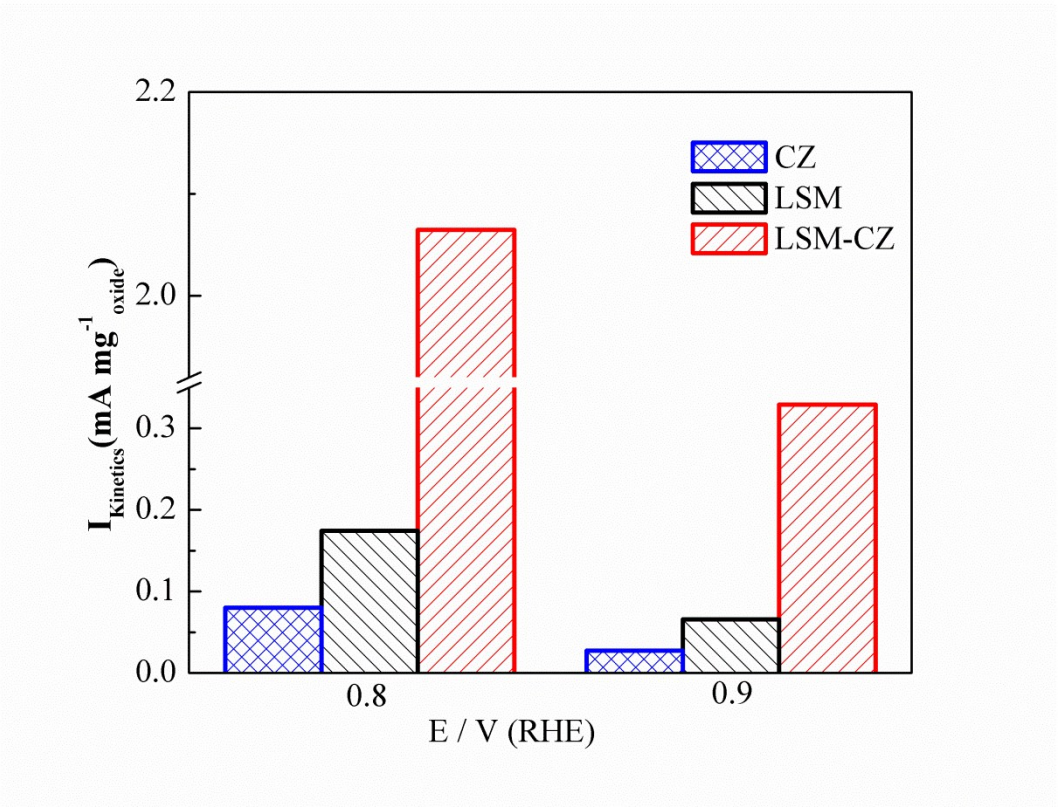

Figure S8. Mass specific activities of CZ, LSM, LSM-CZ catalysts at the potential of 0.8 and 0.9 V, respectively.

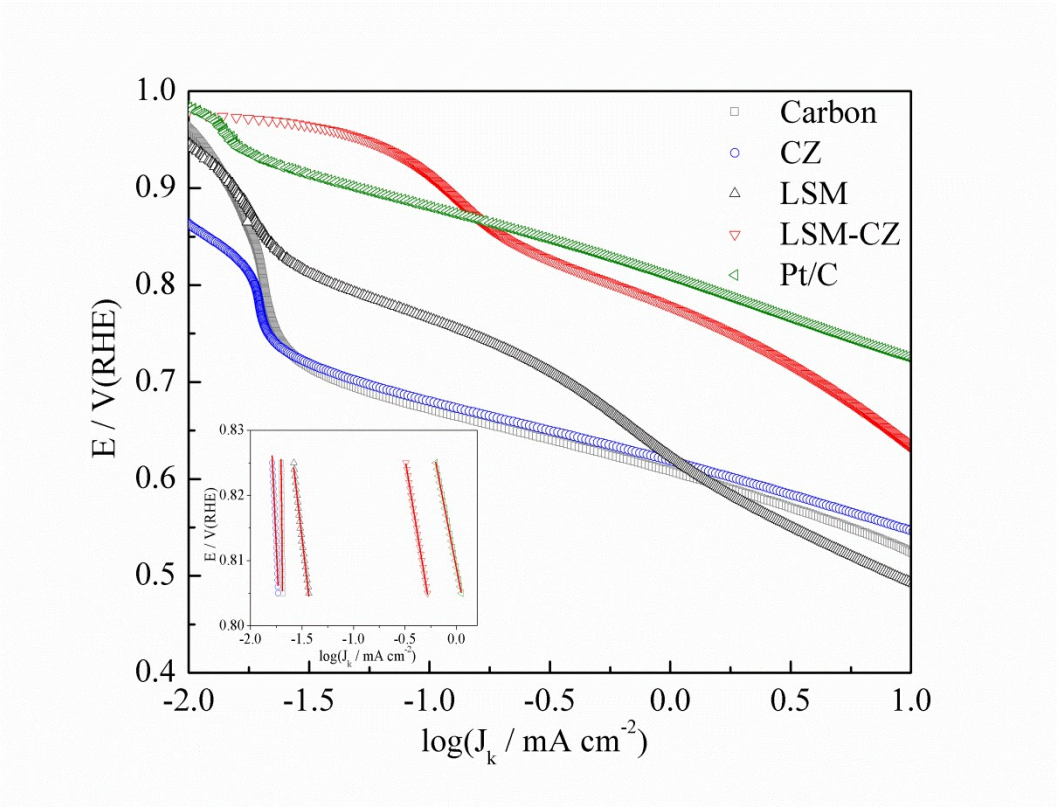

Figure S9. Tafel plots of Carbon, CZ, LSM, LSM-CZ and Pt/C catalysts derived from LSV curves.

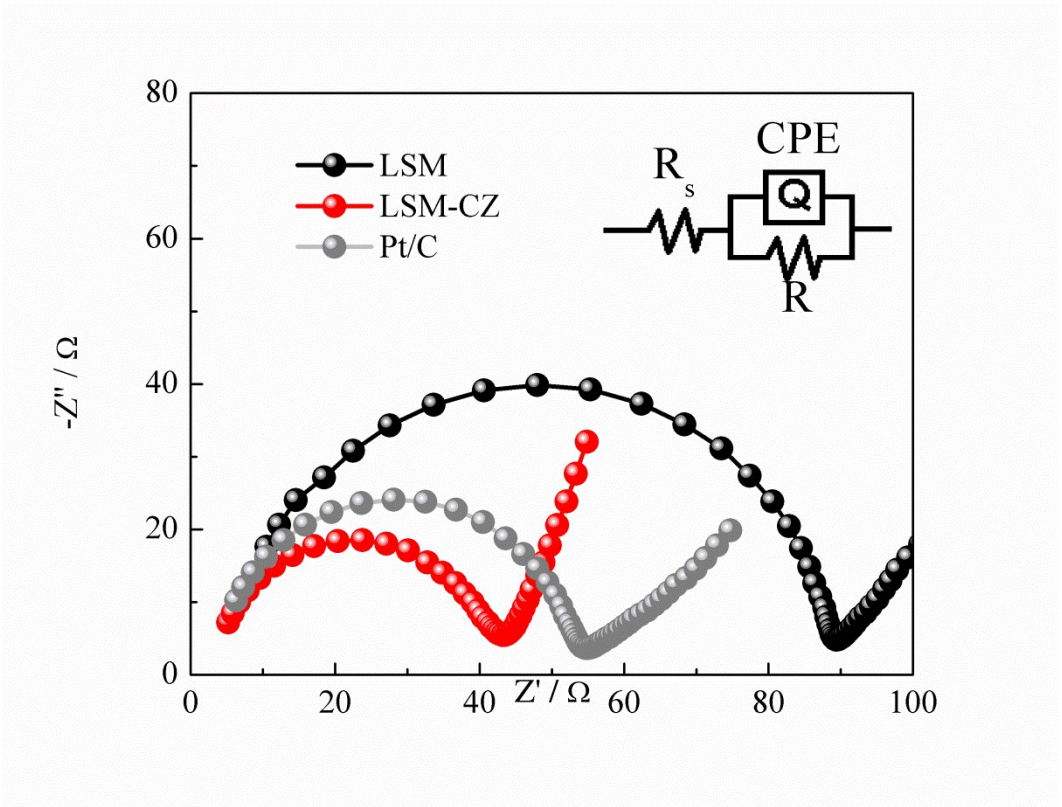

Figure S10. Electrochemical impedance spectra (EIS) of LSM, LSM-CZ and Pt/C.

A

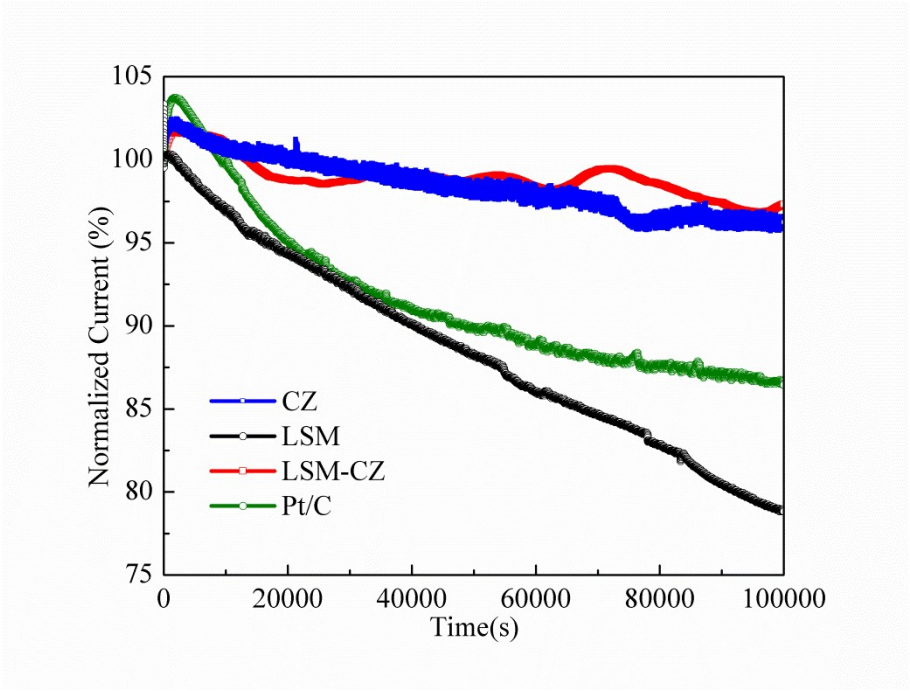

B

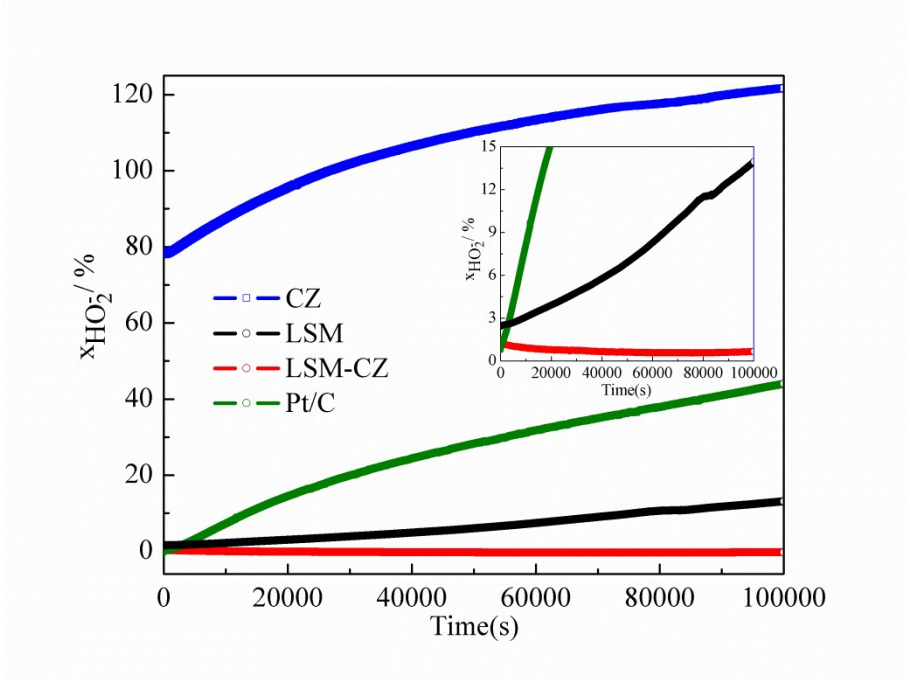

Figure S11. Durabilities (A) and percentages of the peroxides ($X_{HO_2^-}$) (B) of CZ, LSM, LSM-CZ and Pt/C catalysts at 0.4 V in O_2-saturated 0.1 M KOH at the rotating rate of 1600 rpm for 100000 seconds.

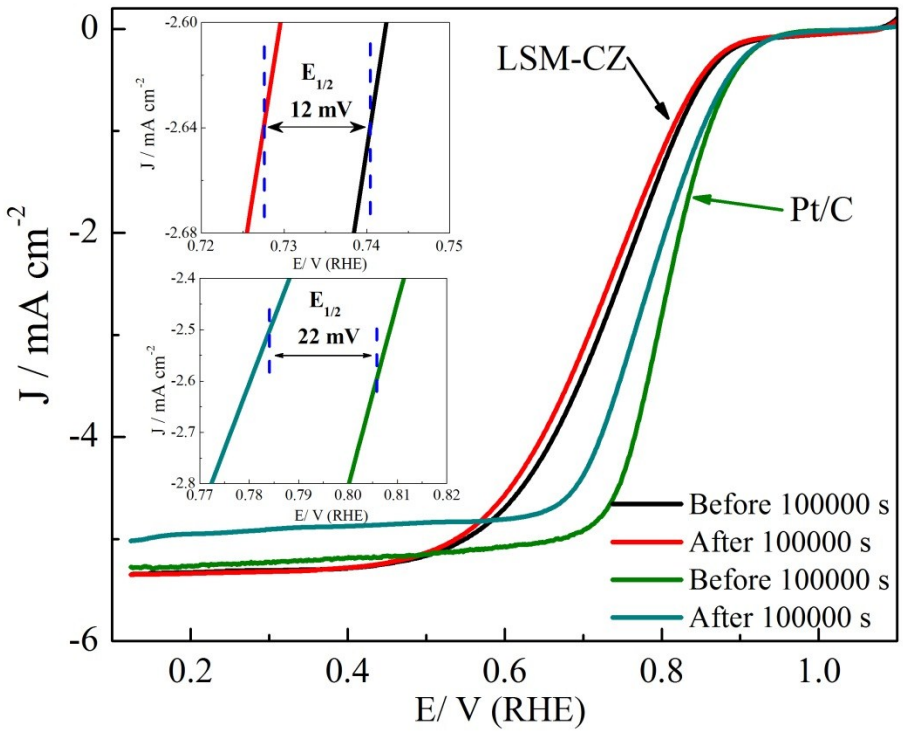

Figure S12. LSV curves of the LSM-CZ and Pt/C samples before and after the aging test for100000 s.

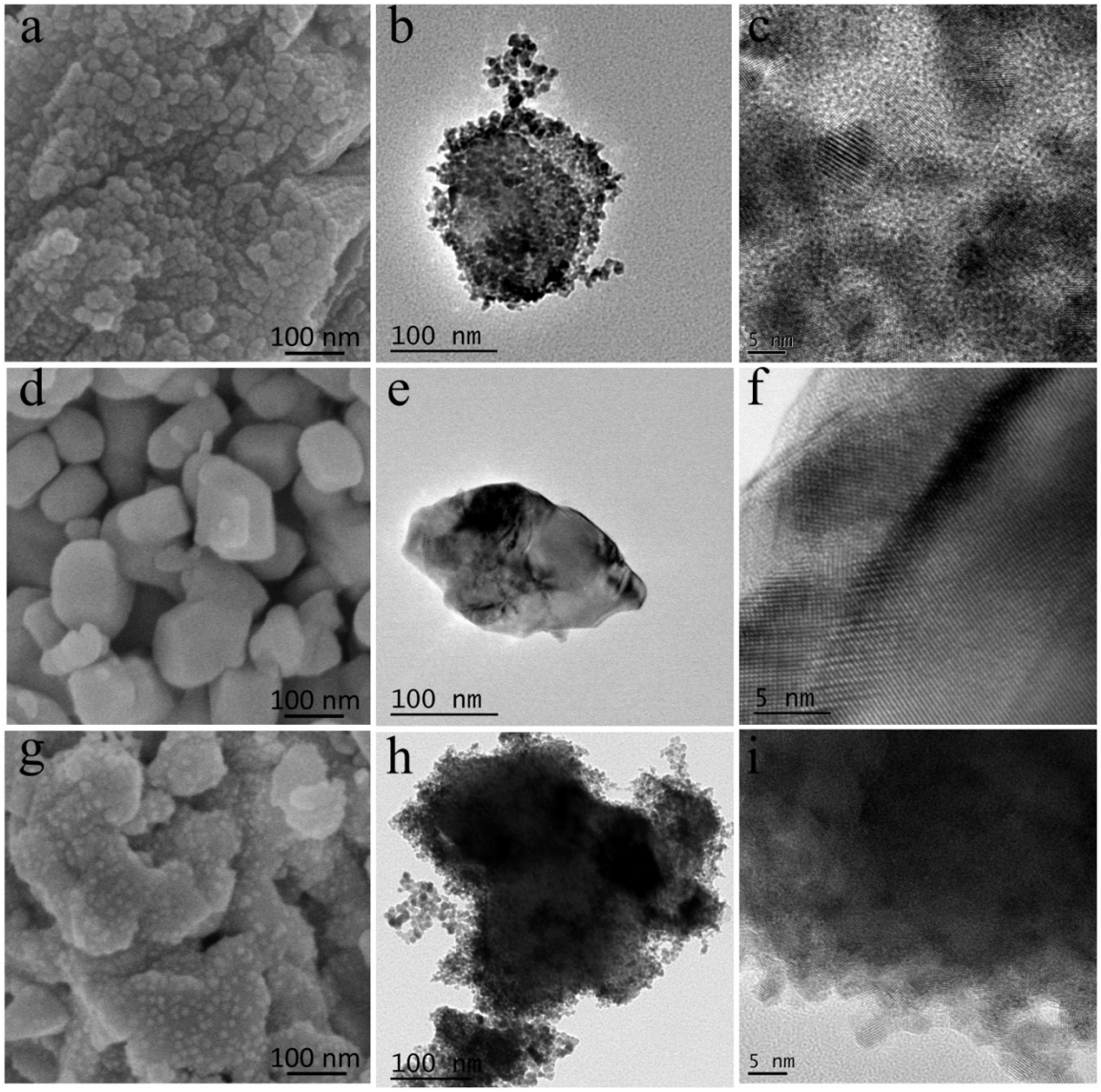

Figure S13. SEM, TEM and high resolution TEM (HRTEM) images of CZ (a~c), LSM (d~f) and LSM-CZ (g~i).

A

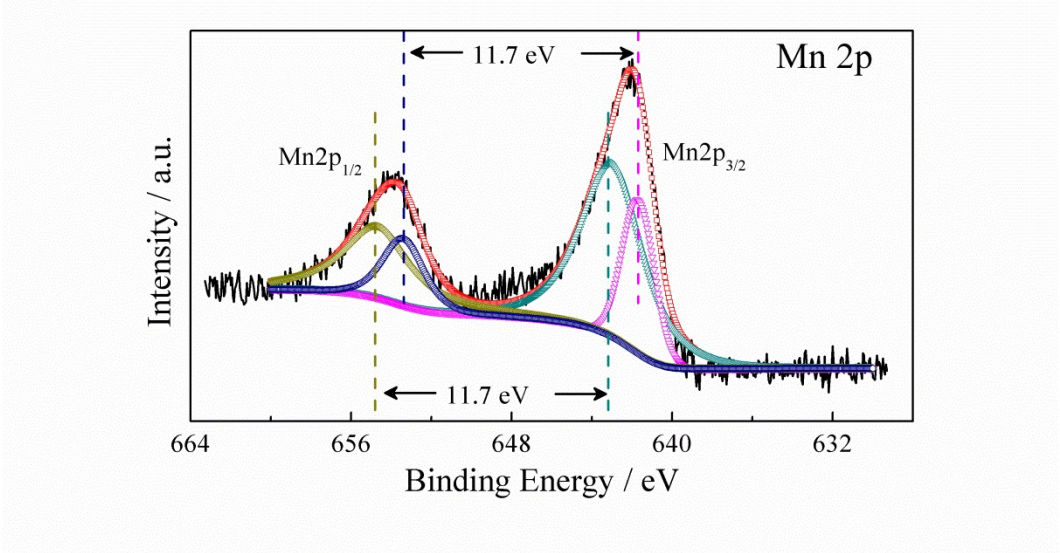

B

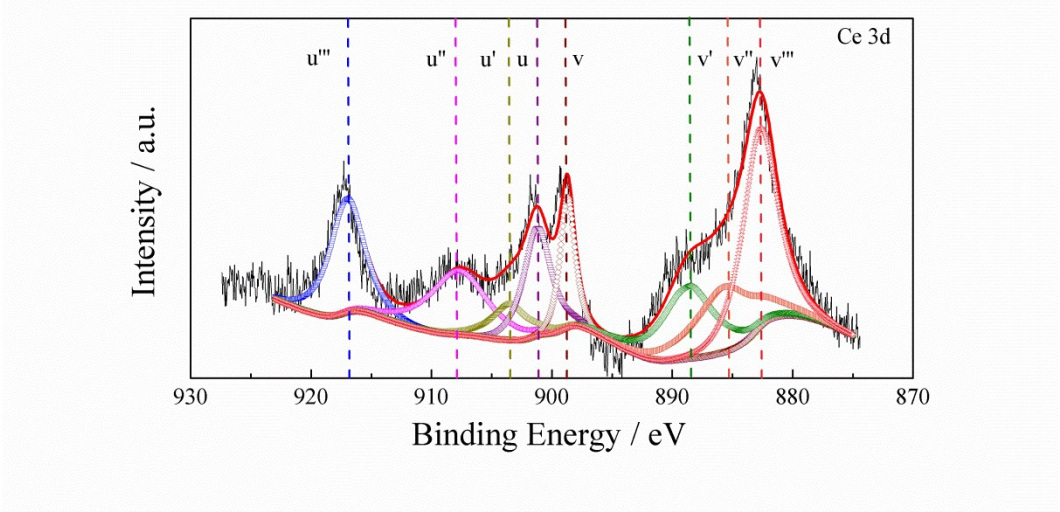

Figure S14. XPS spectra of the Mn 2p (A) and Ce 3d (B) of LSM-CZ.

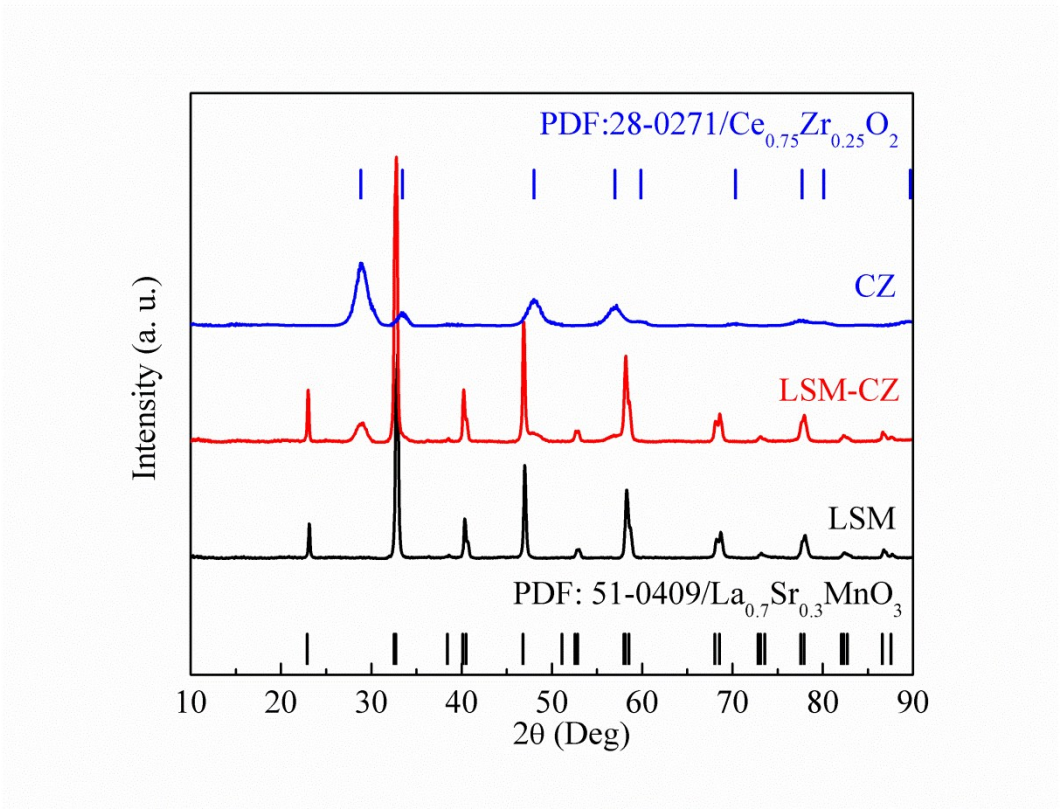

Figure S15. XRD patterns of CZ, LSM and LSM-CZ.

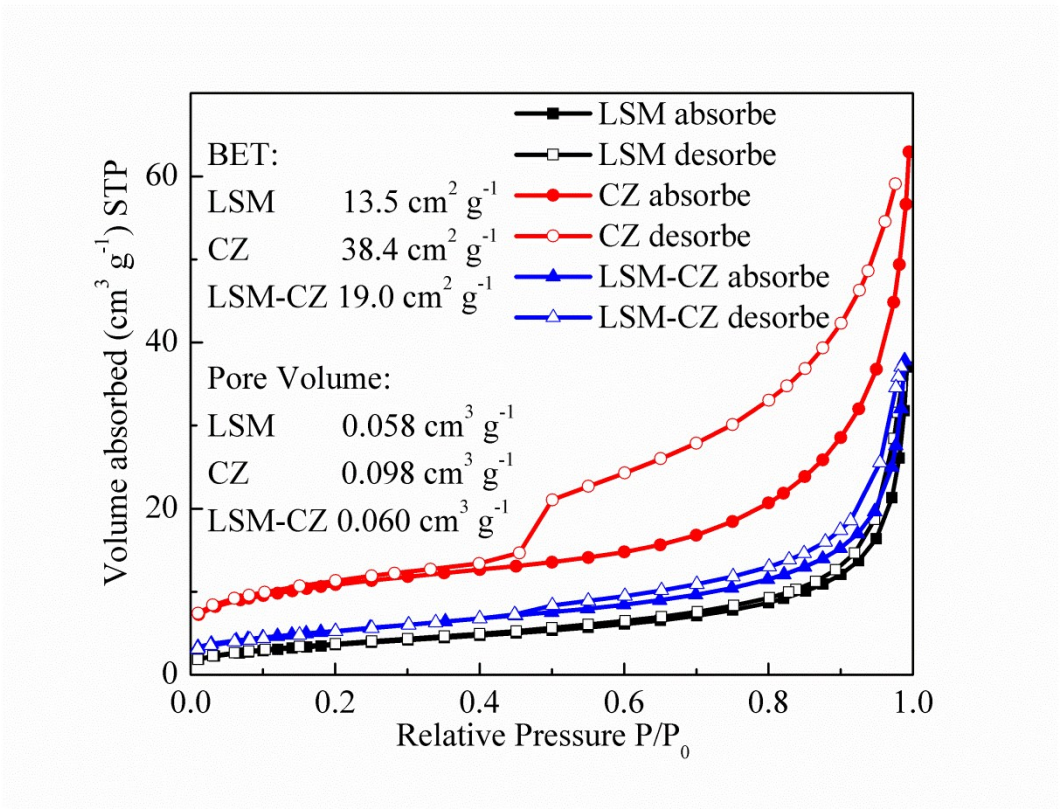

Figure S16. Nitrogen adsorption/desorption isotherms of CZ, LSM and LSM-CZ. The Brunauer-Emmett-Teller (BET) surface areas and pore volumes of these samples are shown in the inset of the figure. .

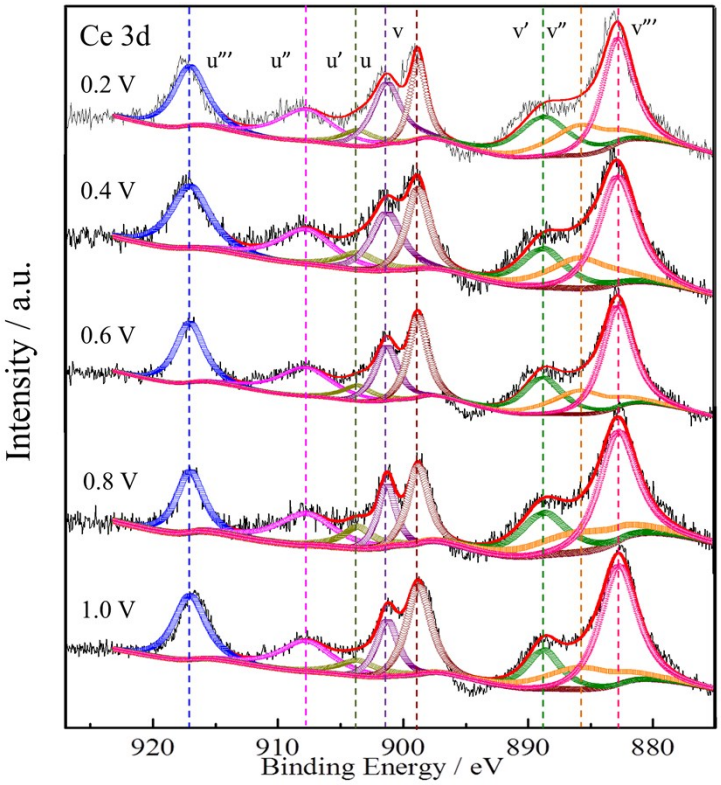

Figure S17. XPS spectra of Ce 3d of LSM-CZ in the scanning potential range from 1.0 V to 0.2 V.

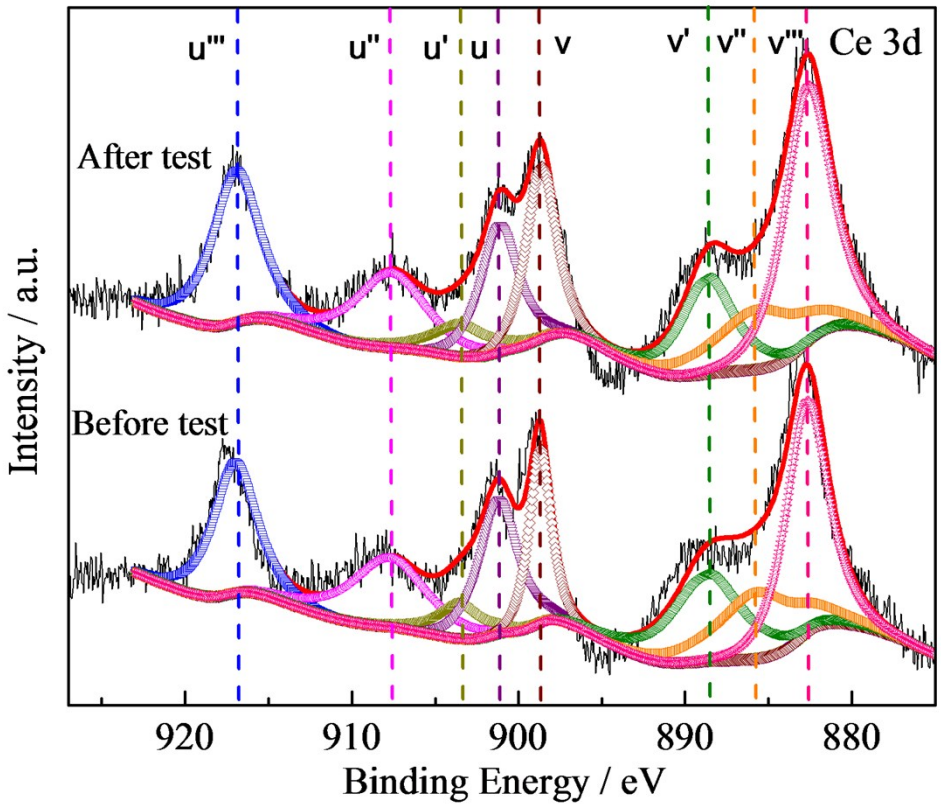

Figure S18. XPS spectra of Ce 3d of LSM-CZ before and after the degradation test.

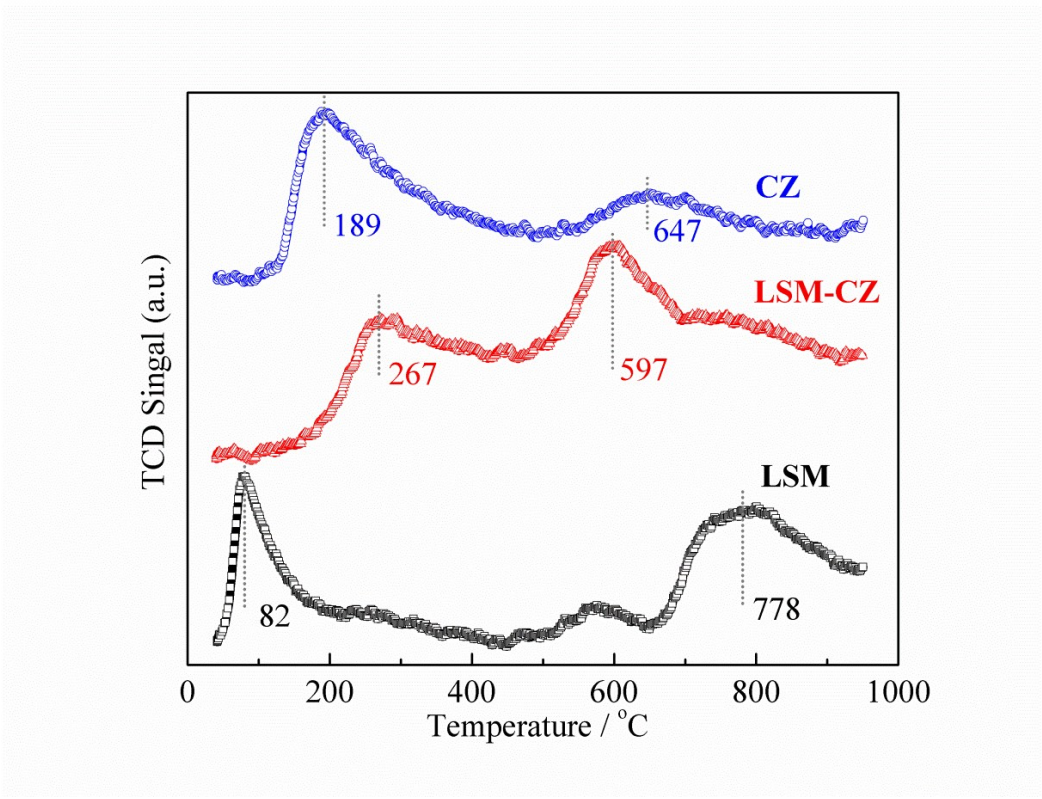

Figure S19. Oxygen-temperature programmed desorption (O-TPD) patterns of LSM, CZ and LSM-CZ.

Table S1 ICP-MS results of the LSM and LSM-CZ samples.

Sample	La (mol %)	Sr (mol %)	Mn (mol %)	Ce (mol %)	Zr (mol %)	Stoichiometry
LSM	35.02	14.98	50	0	0	$La_{0.7}Sr_{0.3}MnO_3$
LSM-CZ	29.21	12.45	41.66	12.53	4.15	$La_{0.701}Sr_{0.299}MnO_3$-$Ce_{0.751}Zr_{0.249}$

Table S2. I-V/I-P curves of the Mg/Al air batteries using as LSM and LSM-CZ as ORRCs.

Cell Style	Catalyst	Electrolyte	Temperature / ^{o}C	OCV	P_{max} / mW cm^{-2}
Mg-Air	LSM	10wt% NaCl	25±1	1.519	63.7±3
	LSM-CZ			1.527	91.5±3
Al-Air	LSM	4 mol/L KOH	36±2	1.575	155.6±5
	LSM-CZ			1.586	233.4±5

Table S3. Onset potentials (E_{onset}), half-wave potentials ($E_{1/2}$), Tafel slopes, electron transferred number (n_{e-}), kinetics current densities ($I_{kinetics}$) and percent of the HO_2^- (X_{HO2-}) at the potential of 0.4 V of Carbon, CZ, LSM, LSM-CZ and Pt/C catalysts.

Sample	E_{onset} / V (at 100μA cm^{-2})	$E_{1/2}$ / V	n (E1/2)	HO_2-% (E1/2) (from Disk, ring current and N) / %	n (0.3 V) (from Disk, ring current and N)	HO_2-%(0.3 V) (from Disk, ring current and N) / %	n (0.3 V) (from K-L equation)	$I_{kinetics}$/ (mA mg^{-1}oxide) (at 0.8 V)	$I_{kinetics}$ / (mA mg^{-1}oxide) (at 0.9 V)	Tafel slop / mV dec^{-1} (0.80~0.83 V)
Carbon	0.737	0.625	2.41	79.62	2.43	78.71	2.78	/	/	/
CZ	0.729	0.598	2.60	70.13	2.52	74.06	3.28	0.80	0.03	345.2
LSM	0.823	0.584	3.91	4.72	3.91	4.68	3.76	0.17	0.07	134.7
LSM-CZ	0.929	0.740	3.99	0.71	3.98	0.98	4.00	2.06	0.33	95.2
Pt/C	0.938	0.804	3.98	0.89	3.97	1.48	3.92	/	/	80.6

Table S4. Onset potential (E_{onset}), half-wave potential ($E_{1/2}$), limitting current density (J_{lim}) of the perovskites stemmed from $LaMnO_3$ in the literatures and this work.

Sample	Electrolyte	J_{lim} (mA cm^{-2}) 1600rpm	$E_{onset\ potential}$ (V) (vs. RHE, 100 μA cm^{-2})	$E_{1/2}$ (V) (vs. RHE)	Catalyst loading (μg cm^{-2})	Oxide loading (μg cm^{-2})	Refences	Remarks
$La_{0.7}Sr_{0.3}MnO_3$ -$Ce_{0.75}Zr_{0.25}O_2$	0.1mol/L KOH	5.4	**0.929**	0.740	471.8	235.9	**This work**	
$La_{0.7}Sr_{0.3}MnO_3$		5.4	0.823	0.584				
$LaMnO_{3+\delta}$		/	**0.92** [e]	/				
$La_{0.5}Ca_{0.5}MnO_3$		/	0.88 [e]	/				
$LaMnO_3$	0.1mol/L KOH	/	0.834 [e]	/	300	250	1	
$LaMn_{0.5}Cu_{0.5}O_3$		/	0.781 [e]	/				
$LaMn_{0.5}Ni_{0.5}O_3$		/	0.80	/				
Co-OEP/LSMF/C	0.1mol/L KOH	4.0 [b]	**0.906** [f]	0.78	199	49.7	2	
$LaMnO_{3+\delta}$	0.1mol/L KOH	/	**0.89**	/	300	250	3	
	0.1mol/L NaOH	/	0.855	/				
	0.1mol/L LiOH	/	0.825	/				
$LaMnO_3$	0.1mol/L KOH	5.0	**0.88**	0.74	300	250	4	
$LaMn_{0.9}Co_{0.1}O_3$/NCNT		5.2	**0.878** [β]	0.758 [β]				
$LaMnO_3$	0.1mol/L KOH	4.5	0.728 [β]	0.558 [β]	410	287	5	
$LaMn_{0.9}Co_{0.1}O_3$		4.8	0.728 [β]	0.618 [β]				
$La_{0.8}Sr_{0.2}Mn_{0.6}Ni_{0.4}O_3$		4.43	**0.868** [β]	0.628 [β]				
$La_{0.8}Sr_{0.2}MnO_3$	0.1mol/L KOH	3.28	0.838 [β]	0.618 [β]	168	140	6	
$La_{0.8}Sr_{0.2}Mn_{0.8}Ni_{0.2}O_3$		3.63	0.848 [β]	0.628 [β]				
$Ag/LaMnO_3$	0.1mol/L KOH	5.4	**0.85**	0.725	662.4	509.6	7	
$La_{0.8}Sr_{0.2}MnO_3$ Nanorod	0.1mol/L KOH	6.3 [d]	**0.834** [γ]	0.66 [γ]	/	/	8	
$La_{0.8}Sr_{0.2}MnO_3$ Particle		2.95 [d]	0.785 [γ]	0.638[γ]	/	/		
HS-$La_{0.8}Sr_{0.2}MnO_3$		6.46 [d]	**0.827** [γ]	0.638 [γ]				
C-$La_{0.8}Sr_{0.2}MnO_3$	0.1mol/L KOH	4.94 [d]	0.765 [γ]	0.602 [γ]	401.3	200.65	9	
U-$La_{0.8}Sr_{0.2}MnO_3$		5.14 [d]	0.78 [γ]	0.609 [γ]				
$LaMnO_3$ film	0.1mol/L KOH	/	**0.825** [e]	/	/	/	10	
$La_{0.67}Sr_{0.33}MnO_3$ film		/	0.825 [e]	/	/	/		
$LaMnO_3$/GR	0.1mol/L KOH	3.8	**0.8**	0.67	51	35.7	11	
$LaMnO_3$/NC		3.3	0.8	0.68				
$La_{0.67}Sr_{0.33}MnO_3$ film	0.1mol/L KOH	/	**0.8**	/	/	/	12	
$LaCa_{0.5}Mn_{0.5}O_3$	0.1mol/L KOH	5.7	**0.78**	/	300	250	13	
$La_{0.4}Sr_{0.6}MnO_3$	0.1mol/L KOH	1.77 [a]	**0.765** [α]	0.465 [α]	108.5	108.5	14	
$La_{0.2}Sr_{0.8}MnO_3$		1.37 [a]	0.665 [α]	0.395 [α]				
$La_{0.8}Sr_{0.2}MnO_3$		1.47[a]	0.565 [α]	0.415 [α]				
$La_{0.6}Sr_{0.4}MnO_3$		1.52 [a]	0.565 [α]	0.415 [α]				
$La_{0.6}Ca_{0.4}MnO_3$ /graphene	0.1mol/L KOH	3.6	**0.765** [α]	0.505 [α]		/		
$LaMnO_3$		1.4	0.645 [α]	0.495 [α]	57	/	15	
$LaMnO_3$/graphene		2.4	0.685 [α]	0.495 [α]		/		
$LaNi_{0.5}Mn_{0.5}O_3$	0.1mol/L KOH	2.40	**0.761** [γ]	0.561 [γ]	190	158.7	16	
$LaMnO_3$		2.35	0.711 [γ]	0.541 [γ]				
$La_{0.8}Sr_{0.2}MnO_3$	0.1mol/L KOH	4.5	**0.746** [γ]	0.606 [γ]	655	327.5	17	
$La_{0.8}Sr_{0.2}MnO_{3-\delta}$ film	0.1mol/L KOH	/	0.73	/	/	/	18	
$LaMn_{0.9}Co_{0.1}O_3$/GR	0.1mol/L KOH	4.6	**0.665** [α]	0.467 [α]	225	125	19	
$LaMn_{0.85}Co_{0.15}O_3$/GR		4.3	0.665 [α]	0.464 [α]				
$LaMnO_3$/GR		2.9	0.575 [α]	0.395 [α]				
$LaMn_{0.95}Co_{0.05}O_3$/GR		3.6	0.595 [α]	0.425 [α]				
1%Ag/$LaMnO_3$-RGO		4.3	**0.775** [α]	0.545 [α]				
2%Ag/$LaMnO_3$-RGO		5.45	0.775 [α]	0.565 [α]				
4%Ag/$LaMnO_3$-RGO		4.51	0.775 [α]	0.545 [α]				
$LaMnO_3$		3.2	0.655 [α]	0.385 [α]				
$LaMnO_3$-RGO		3.59	0.735 [α]	0.525 [α]				
$La(Co_{0.55}Mn_{0.45})_{0.99}O_3$+ NRGO	0.1mol/L KOH +0.01M $K_3Fe(CN)_6$	6.57 [c]	**0.944**	0.691	1000	850	20	
$La(Co_{0.55}Mn_{0.45})_{0.99}O_3$/ NRGO		6.64 [c]	0.935	0.776			21	

[a,b,c,d] The rotating rate of RDE is 500, 900, 2000 and 2500 rpm, respectively.

[e, f, g] the onset potential derived at 25,40 and 500 μA cm^{-2}, respectively.

[α]: converted from Hg/HgO electrode, E vs RHE = E vs MMO + 0.098 V + 0.059 × pH.

[β]: converted from saturated camel electrode, E vs RHE = E vs SCE + 0.241 V +0.059 × pH.

[γ]: converted from

$La(Co_{0.55}Mn_{0.45})_{0.99}O_3$		5.3 [c]	0.82	0.52			
$La_{0.67}Sr_{0.33}MnO_3$ film		/	**0.85** [f]	/	/	/	
$La_{0.5}Sr_{0.5}MnO_3$ film		/	0.83 [f]	/	/	/	
$La_{0.8}Sr_{0.2}MnO_3$ film	0.1mol/L KOH	/	0.82 [f]	/	/	/	
$LaMnO_3$ film	+10 mM $K_4Fe(CN)_6$	/	0.74 [f]	/	/	/	22
$La_{0.9}Sr_{0.1}MnO_3$ film		/	0.78 [f]	/	/	/	
$La_{0.3}Sr_{0.7}MnO_3$ film		/	0.73 [f]	/	/	/	
$La_{0.8}Sr_{0.2}MnO_3$	1mol/L KOH	2.15 [b]	**0.93**	0.81	217	180	23
$La_{0.8}Sr_{0.2}MnO_3$		2.3 [b]	0.9	0.825	911	91	
$LaMnO_3$/C		3.2	**0.92**	0.82	771.1	385.6	24
$LaMnO_3$	1mol/L NaOH	2.8	**0.917** [β]	0.827 [β]	5:2		25
		2.2	0.877 [β]	0.787 [β]	4:1		
		2.2	0.887 [β]	0.777 [β]	2:1		
		1.8	0.887 [β]	0.767 [β]	7:4		
$La_{0.8}Sr_{0.2}MnO_3$/CNT	1mol/L KOH	3.4	**0.89**	0.81	170	34	26
$La_{0.9}Sr_{0.1}MnO_3$/CNT		3.2	0.87	0.77		28.9	
Vulcan-$LaMnO_3$		2.1 [b]	**0.88**	0.76			
$LaMnO_3$	1mol/L KOH	1.1 [b]	0.72	0.64	83	46	27
$LaMnO_3$-AC/C		1.9 [b]	0.85	0.72			
$LaMnO_3$-SG/C		2.1 [b]	0.85	0.75			
$La_{0.8}Sr_{0.2}MnO_3$	1mol/L KOH	3.3	**0.88** [g]	0.82	/		
	1mol/LKOH +0.1mol/L EG 353K	3.2	0.87 [g]	0.81	/	1000	28
$La_{0.8}Sr_{0.2}MnO_3$	1mol/L NaOH	2.3 [b]	**0.87**	0.79	128	91	29
$La_{0.8}Sr_{0.2}MnO_3$		2.1 [b]	0.86	0.76	65	46	
$La_{0.6}Ca_{0.4}Co_{0.5}Mn_{0.5}O_{3-x}$/C	1mol/L KOH	3.4	**0.864** [α]	0.744 [α]	101.9	/	30
$La_{0.6}Ca_{0.4}Co_{0.5}Mn_{0.5}O_{3-x}$		2.2	0.744 [α]	0.604 [α]		/	
$La_{0.8}Sr_{0.2}MnO_3$ film	1mol/L KOH	/	**0.78**	/	/	/	31
$LaMnO_3$ film		/	0.75	/	/	/	

[1] J. Suntivich, H. A. Gasteiger, N. Yabuuchi, H. Nakanishi, J. B. Goodenough, Y. Shao-Horn, *Nature chemistry* **2011**, *3*, 546-550
[2] T. Nagai, S.-i. Yamazaki, M. Asahi, Z. Siroma, N. Fujiwara, T. Ioroi, *Journal of Power Sources* **2015**, *293*, 760-766
[3] J. Suntivich, E. E. Perry, H. A. Gasteiger, Y. Shao-Horn, *Electrocatalysis* **2012**, *4*, 49-55
[4] V. Celorrio, E. Dann, L. Calvillo, D. J. Morgan, S. R. Hall, D. J. Fermin, *ChemElectroChem* **2016**, 3, 283-291
[5] D. U. Lee, M. G. Park, H. W. Park, M. H. Seo, V. Ismayilov, R. Ahmed, Z. Chen, *Electrochemistry Communications* **2015**, *60*, 38-41
[6] Z. Wang, Y. You, J. Yuan, Y. X. Yin, Y. T. Li, S. Xin, D. Zhang, *ACS applied materials & interfaces* **2016**, *8*, 6520-6528
[7] S. A. Park, E. K. Lee, H. Song, Y. T. Kim, *Scientific reports* **2015**, *5*, 13552
[8] F. Lu, Y. Wang, C. Jin, F. Li, R. Yang, F. Chen, *Journal of Power Sources* **2015**, *293*, 726-733
[9] F. Lu, J. Sui, J. Su, C. Jin, M. Shen, R. Yang, *Journal of Power Sources* **2014**, *271*, 55-59
[10] K. A. Stoerzinger, M. Risch, J. Suntivich, W. M. Lü, J. Zhou, M. D. Biegalski, H. M. Christen, Ariando, T. Venkatesan, Y. Shao-Horn, *Energy & Environmental Science* **2013**, *6*, 1582
[11] W. G. Hardin, J. T. Mefford, D. A. Slanac, B. B. Patel, X. Wang, S. Dai, X. Zhao, R. S. Ruoff, K. P. Johnston, K. J. Stevenson, *Chemistry of Materials* **2014**, *26*, 3368-3376
[12] D. Kan, Y. Orikasa, K. Nitta, H. Tanida, R. Kurosaki, T. Nishimura, T. Sasaki, H. Guo, Y. Ozaki, Y. Uchimoto, Y. Shimakawa, *The Journal of Physical Chemistry C* **2016**, *120*, 6006-6010
[13] J. Suntivich, H. A. Gasteiger, N. Yabuuchi, Y. Shao-Horn, *Journal of The Electrochemical Society* **2010**, *157*, B1263
[14] J. Tulloch, S. W. Donne, *Journal of Power Sources* **2009**, *188*, 359-366
[15] J. Hu, L. Wang, L. Shi, H. Huang, *Journal of Power Sources* **2014**, *269*, 144-151
[16] J. Sunarso, A. A. J. Torriero, W. Zhou, P. C. Howlett, M. Forsyth, *The Journal of Physical Chemistry C* **2012**, *116*, 5827-5834
[17] C. Jin, X. Cao, L. Zhang, C. Zhang, R. Yang, *Journal of Power Sources* **2013**, *241*, 225-230
[18] M. Risch, K. A. Stoerzinger, S. Maruyama, W. T. Hong, I. Takeuchi, Y. Shao-Horn, *Journal of the American Chemical Society* **2014**, *136*, 5229-5232

[19] J. Hu, L. Wang, L. Shi, H. Huang, *Electrochimica Acta* **2015**, *161*, 115-123
[20] J. Hu, L. Shi, Q. Liu, H. Huang, T. Jiao, *RSC Adv.* **2015**, *5*, 92096-92106
[21] X. Ge, F. W. Goh, B. Li, T. S. Hor, J. Zhang, P. Xiao, X. Wang, Y. Zong, Z. Liu, *Nanoscale* **2015**, *7*, 9046-9054
[22] K. A. Stoerzinger, W. Lu, C. Li, Ariando, T. Venkatesan, Y. Shao-Horn, *The journal of physical chemistry letters* **2015**, *6*, 1435-1440
[23] T. Poux, F. S. Napolskiy, T. Dintzer, G. Kéranguéven, S. Y. Istomin, G. A. Tsirlina, E. V. Antipov, E. R. Savinova, *Catalysis Today* **2012**, *189*, 83-92
[24] T. Li, J. Liu, X. Jin, F. Wang, Y. Song, *Electrochimica Acta* **2016**, *198*, 115-126
[25] J. Liu, X. Jin, W. Song, F. Wang, N. Wang, Y. Song, *Chinese Journal of Catalysis* **2014**, *35*, 1173-1188
[26] K. Miyazaki, K.-i. Kawakita, T. Abe, T. Fukutsuka, K. Kojima, Z. Ogumi, *J. Mater. Chem.* **2011**, *21*, 1913-1917
[27] G. Kéranguéven, S. Royer, E. Savinova, *Electrochemistry Communications* **2015**, *50*, 28-31
[28] K. Miyazaki, N. Sugimura, K. Matsuoka, Y. Iriyama, T. Abe, M. Matsuoka, Z. Ogumi, *Journal of Power Sources* **2008**, *178*, 683-686
[29] T. Poux, A. Bonnefont, G. Kerangueven, G. A. Tsirlina, E. R. Savinova, *Chemphyschem : a European journal of chemical physics and physical chemistry* **2014**, *15*, 2108-2120
[30] S. Malkhandi, P. Trinh, A. K. Manohar, K. C. Jayachandrababu, A. Kindler, G. K. Surya Prakash, S. R. Narayanan, *Journal of the Electrochemical Society* **2013**, *160*, F943-F952
[31] Y. Miyahara, K. Miyazaki, T. Fukutsuka, T. Abe, *Journal of the Electrochemical Society* **2014**, *161*, F694-F697